Slow relaxation of cascade-induced defects in Fe

Laurent Karim Béland, Yuri N. Osetsky, Roger E. Stoller, and Haixuan Xu

Slow relaxation of cascade-induced defects in Fe

Laurent Karim Béland,[1] Yuri N. Osetsky,[1] Roger E. Stoller,[1] and Haixuan Xu[2], *

[1]*Materials Science and Technology Division, Oak Ridge National Laboratory, Oak Ridge, Tennessee 37831-6138, USA*
[2]*Department of Materials Science, University of Tennessee, Knoxville, TN, USA*
(Dated: January 30, 2015)

On-the-fly kinetic Monte Carlo (KMC) simulations are performed to investigate slow relaxation of non-equilibrium systems. Point defects induced by 25 keV cascades in α-Fe are shown to lead to a characteristic time-evolution, described by the *replenish and relax* mechanism. Then, we produce an atomistically-based assessment of models proposed to explain the slow structural relaxation by focusing on the aggregation of 50 vacancies and 25 self-interstitial atoms (SIA) in 10-lattice-parameter α-Fe boxes, two processes that are closely related to cascade annealing and exhibit similar time signature. Four atomistic effects explain the timescales involved in the evolution: defect concentration heterogeneities, concentration-enhanced mobility, cluster-size dependent bonding energies and defect-induced pressure. These findings suggest that the two main classes of models to explain slow structural relaxation, the Eyring model and the Gibbs model, both play a role to limit the rate of relaxation of these simple point-defect systems.

I. INTRODUCTION

Slow physical aging, which occurs over several orders of magnitude in time, is ubiquitous in disordered materials, such as glasses [1–3], cellulose [4], colloids [5–8], proteins [9–11], gelatin gels [12], polymers [13], amorphous solids [14, 15] and concrete [16, 17]. Plotting the variables describing structural relaxation (e.g. potential energy, stress or other order parameters) of these off-equilibrium systems as a function of the logarithm of time results in a roughly linear trend, i.e. these systems relax over logarithmic timescales. For simplicity, the term logarithmic relaxation is used to describe this behavior.

Most models describe such aging as a sequence of activated processes that permit relaxation. As the system relaxes, the energy barriers of these processes increase , which delays aging by growing orders of magnitude in time. The literature contains a large number of such propositions.

For example, in the Eyring model [18], barriers are linked to the energy recovered during relaxation through their coupling to shear strain. This idea, where the degree of relaxation has an effect on the height of the barriers, has been adapted and modified to include hierarchically constrained dynamics [19], stress relaxation in the Burridge-Knopoff model [20], models with a stress-induced barrier increase [15, 21] and glassy polymer relaxation [13, 22] after nano-indentation. We present a simplified illustration of the Eyring model in Fig. 1. In this paper, we will also consider other mechanism based on a feedback between the state of relaxation and the waiting time as variations on the Erying model.

On the other hand, the Gibbs model [23] and its variants [24–26] argue that the system initially possesses a distribution of relaxation events with a near-constant density as a function of activation barrier, or rates de-
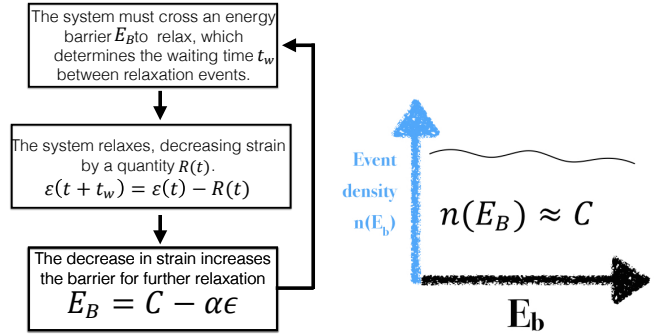

FIG. 1. Left panel: A simplified illustration of the Eyring model. The state of relaxation (in this case, strain), acts on the activation barrier, causing a feedback loop, slowing down relaxation. Right panel: An illustration of the density of relaxation events $n(E_B)$ as a function of energy barrier E_B as proposed in the Gibbs model. It is approximately constant, which leads to logarithmic relaxation.

scribed by a multiplicative stochastic process [3], which leads to logarithmic relaxation. A newly proposed model links logarithmic time-evolution to the system moving from one local state to another, where the waiting time of each state is defined by a power law and where all states evolve simultaneously [27]. We present a simplified illustration of the density distribution put hypothesized by the Gibbs model in Fig. 1.

Recently, a novel description of logarithmic relaxation was proposed, coined *replenish and relax* [28], which was based on nanocalorimetric measurements combined with the kinetic Activation Relaxation Technique (k-ART) [29, 30] simulations of the annealing of ion-implanted *c*-Si. In this slightly disordered system, it was showed that relaxation is caused by the aggregation, reconfiguration and annihilation of small point-defect clusters [31].

In the *replenish and relax* model, relaxation takes place by executing events that lead to deeper energy states, more or less uniformly distributed in activation energy.

* xhx@utk.edu

The energy landscape depletes all the events with a barrier low enough to be accessible for a given waiting time (the *relax* phase). A high-energy barrier must eventually be crossed to access a new region of the energy landscape with a *replenished* distribution of relaxation events. For such a model to explain long-time relaxation, the barriers to *replenish* the landscape must progressively increase, while the barriers of the events directly related to potential energy minimization must be uncorrelated to this increase.

Isothermal magnetic relaxation measurements of neutron-irradiated Fe also exhibit such long-time relaxation [32]. Work concerning a related problem, the aggregation of vacancies in α-Fe [33–36] showed that the transition from a state involving mostly mono vacancies to a state with large clusters involves logarithmic decay that is well described by the *replenish and relax* model. These simulations in Fe and Si provided an accurate description of the microscopic processes, but did not explain why the barriers to unlock relaxation were increasing.

Typically, defect-evolution in irradiated Fe is modeled by assigning a few diffusion and reaction rates to each type of defect (mono-SIA,di-SIA,tri-SIA,tetra-SIA, ..., or mono-vacancies, di-vacancies, tri-vacancies, tetra-vacancies, planar defects, and so on), neglecting most elastic interactions and the effects of minute atomistic reconfigurations. Using this model, four stages (see, e.g. Ref. [37]) are identified to explain the defect kinetics in irradiated Fe, each with their own specific reaction rates. This model adequately explains the sharp features of isochronal annealing after electron irradiation. It shows that atomistic modeling can provide good information about the reaction rates. However, this picture does not correctly explain relaxation after neutron irradiation [32], where such sharp features are absent. On the other hand, molecular-dynamics-generated displacement cascades produce damage more similar to that of neutron and ion irradiation than to that of electron irradiation. Thus, a close look at the time-evolution of such defects, using accelerated dynamics simulations, should shed light on this important problem.

We note that molecular dynamics (MD) simulations were used to explore logarithmic relaxation [10, 11, 38–40] and provide atomistically-base evidence to support models predicting such time-evolution, but this method is severely limited in the range of time-evolution it can reach. These simulations also focus on highly complex materials, such as polymer glasses and proteins, while we are interested in understanding how the interaction of simple point defects can lead to similar kinetics, where the drivers of relaxation can be identified with more confidence.

In this article, we provide novel evidence that logarithmic decay appears in off-equilibrium, albeit largely crystalline, systems through the interaction of point defects. Firstly, we show that the annealing of 25 keV cascades in α-Fe leads to such relaxation over seven orders of magnitude in time. To complete the picture

drawn by vacancy clustering in Fe and cascade annealing, which involves both vacancies and interstitials, we also present simulations of self-interstitial atom (SIA) clustering, that exhibit near-logarithmic behavior over 19 orders of magnitude in time. Secondly, we verify that these systems are described by *replenish and relax*. Thirdly, we examine the drivers of this behavior in the simplest cases, vacancy and interstitial clustering, and identify four mechanisms that explain the gradual increase of barriers during relaxation: defect concentration heterogeneities, concentration-enhanced mobility, cluster-size dependent bond energies and defect-induced pressure. We determine if these mechanisms are related to the Eyring or to the Gibbs model.

II. METHODOLOGY

Molecular dynamics (MD) was used to simulate a 25 keV cascade in Fe. After 15 ps, we extracted the atomic positions of 250000 atoms from the MD and used them as the starting point for on-the-fly KMC simulations at 650K. For these calculations, we use the Self-Evolving Kinetic Monte Carlo (SEAKMC) [41, 42], an off-lattice, on-the-fly kinetic Monte Carlo method that has been shown to accurately simulate the time-evolution of defects in Fe, such as the aggregation of vacancies [34], as well as collisions and transformations of interstitial loops [43].

To simulate the aggregation of SIAs, we replace 25 lattice-sites by $< 110 >$ dumbells in a 2000-atom Fe crystal, for a total of 2025 atoms. The system is simulated at 100 K for times reaching up to 10000 seconds, using the Marinica2007 (M07) [44] potential. We choose a low temperature in order to distinguish the various low-barrier (less than 0.3 eV) processes that lead to interstitial-cluster formation. For this task, we choose the k-ART [29, 30, 45, 46], an off-lattice, self-learning, on-the-fly kinetic Monte Carlo that can exactly handle elastic effects and time-evolution of states interconnected by small-barriers. This algorithm was successfully used to investigate the time-evolution of point defects in c-Si [28, 30, 31], a-Si [30, 47], SiC [48] and Fe [30, 33, 35, 36]. It combines kinetic Monte-Carlo rules [49] to NAUTY [50, 51], a topological analysis software package, and the Activation-Relaxation Technique *nouveau* [45, 52–55].

III. FOUR EXAMPLES OF LOGARITHMIC RELAXATION

The time-evolution for the 25 keV cascade annealing and SIA clustering is plotted in Fig. 2. We also show, for reference, the time-evolution of 50-vacancies aggregating and the annealing of 3 keV ion-implanted c-Si. In all cases, we see that the potential energy relaxation takes place over logarithmic timescales. For reference, we also performed SIA-cluster aggregation runs with the Ackland2004 (A04) [56] potential; the results were similar to
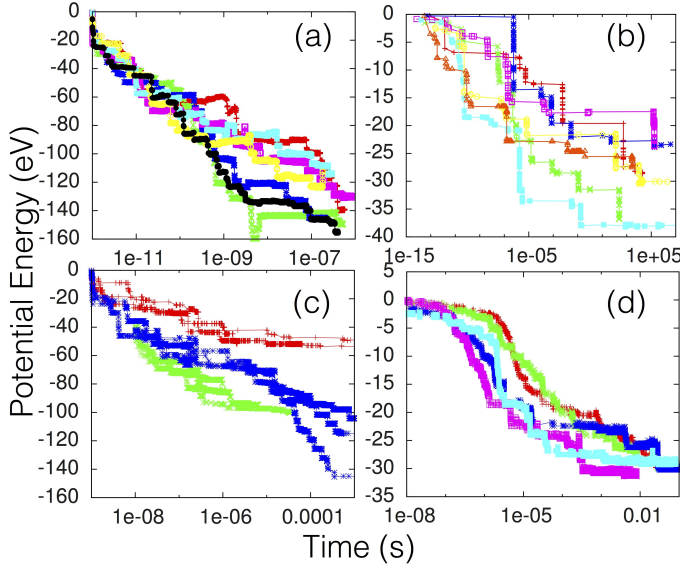
FIG. 2. Time evolution of potential energy of four systems: 25 keV cascade annealing in Fe (a), 25-SIA aggregation in Fe (b), 3 keV c-Si ion implantation annealing (c), and 50-vacancy aggregation in Fe (d).
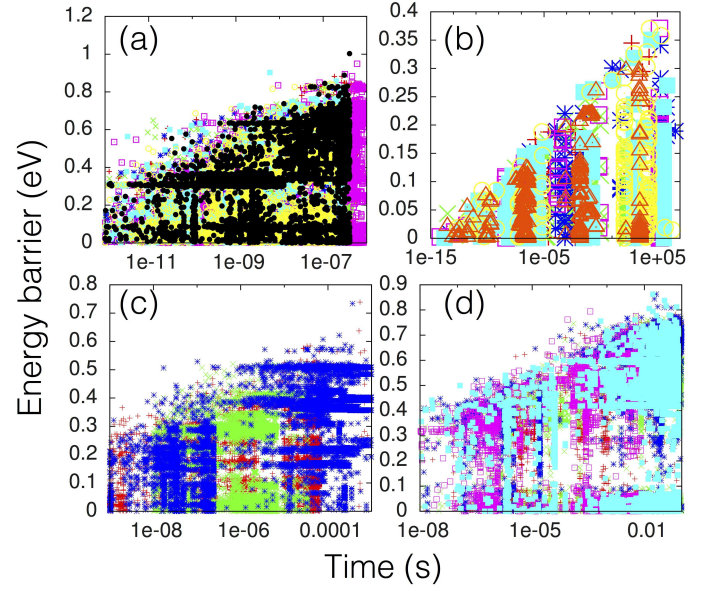

FIG. 3. The activation barriers of the events executed during the simulations: 25 keV cascade annealing in Fe (a), 25-SIA aggregation in Fe (b), 3 keV c-Si ion implantation annealing (c), and 50-vacancy aggregation in Fe (d).

those with the M07 potential, as shown in the Appendix. The variation between each run for the SIA-clustering system is due to each simulation starting from a different random initial configuration. In the Appendix, we show that each of these runs is roughly logarithmic.

We suggest that the reader download and play the movies included in the Supplemental Material [57] in order to visualize the defect evolution in these four systems.

IV. CHARACTERIZING THE POTENTIAL-ENERGY LANDSCAPE: THE GENERALITY OF *REPLENISH AND RELAX*

We plot the activation barriers that were crossed during each of these runs in Fig. 3 . The maximum energy-barrier increases exponentially with time, as expected from Poisson processes, and a wide distribution of barriers is executed in each time-frame. Combined to the fact that potential energy relaxation takes place on a linear scale relative to the number of KMC steps, but logarithmically relative to time, (see Fig. 4 and Fig. 5), this indicates that the largest barriers in each time-frame act as a bottleneck.

Indeed, if low-barrier relaxation events were still available, the residence-time algorithm would have executed them before the high-energy events. One might argue that such high-energy event can be chosen at random, with a low probability, even though low-energy barriers are still present. However, the number of KMC steps between bottleneck events is much too low to attribute selecting these high-barrier events to luck.
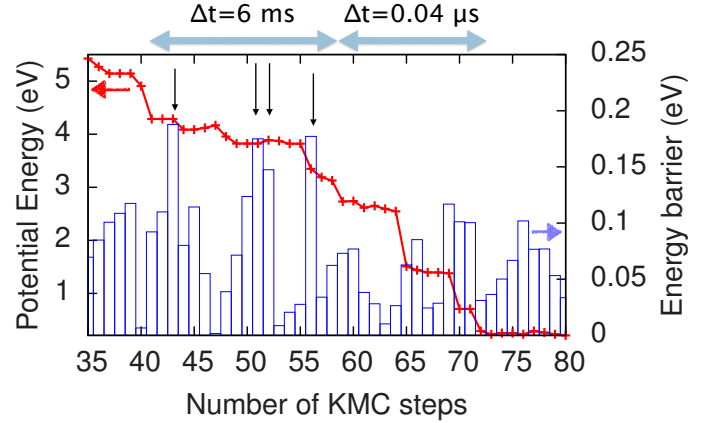

FIG. 4. A representative example of the relaxation kinetics, taken from a 25-SIA run. The black arrows indicate bottleneck events, which account for most of the time-evolution. The blue bars represent the potential energy barrier of each event in the sequence. The red line represents the potential energy of the initial state for each event. The potential energy is shifted relative to that plotted in Fig. 2 for simplicity.

In Fig. 4, we show a typical relaxation sequence. This example is taken from one of the 25-SIA runs. We see two plateaux in potential energy: from KMC step 41 to step 55 and from step 72 to step 80. We also see two rapid decreases in energy (i.e. relaxation phases): from step 25 to step 41 and from step 55 to step 72. The first plateau is characterized by the presence of four large activation barriers, that act as a bottleneck for time-evolution. In contrast, the phases with rapid energy relaxation were executed without crossing large activation barriers. From
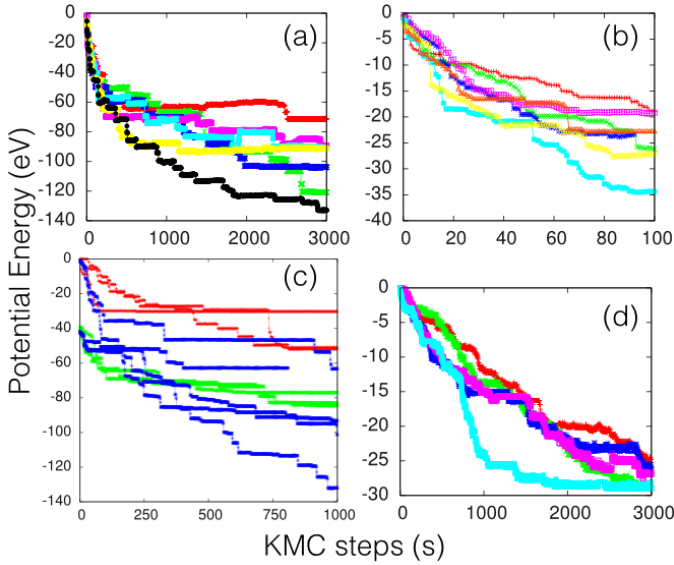
FIG. 5. Evolution of potential energy of four systems as a function of the number of KMC steps : 25 keV cascade annealing in Fe (a), 25-SIA aggregation in Fe(b), 3 keV c-Si ion implantation annealing(c), and 50-vacancy aggregation in Fe(d).
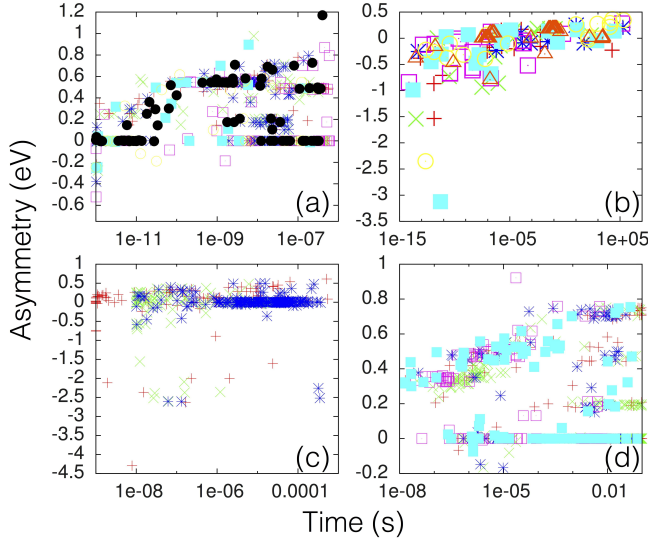

FIG. 6. The difference between the initial and final state of the executed events that have a barrier size in the top-10% of each time-frame, i.e. events corresponding to bottlenecks: 25 keV cascade annealing in Fe (a), 25-SIA aggregation in Fe (b), 3 keV c-Si ion implantation annealing (c), and 50-vacancy aggregation in Fe (d).

a time-evolution perspective, the system took 6 ms to execute events in the first plateau, while it took only 40 ns to execute events in the second relaxation phase.

Generally, the events with large activation barriers do not directly lead to lower-energy states. Instead, they give access to a new region of the potential energy surface were such lower-energy states are accessible by crossing
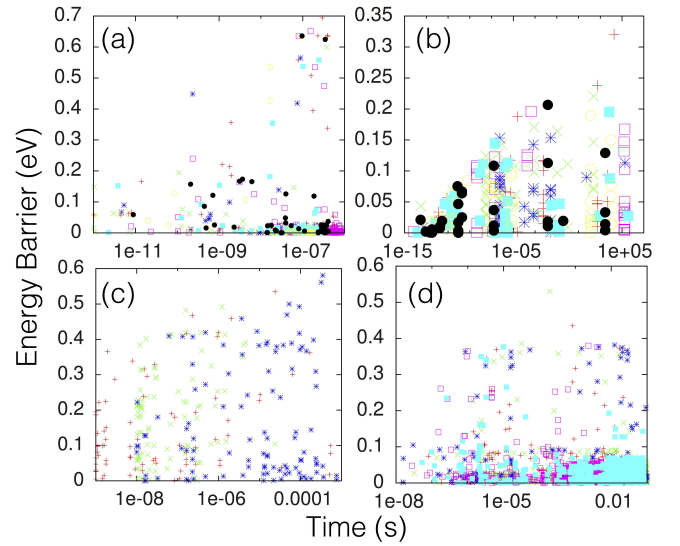

FIG. 7. The barriers of the executed events that permitted large relaxation: 25 keV cascade annealing in Fe (a), 25-SIA aggregation in Fe (b), 3 keV c-Si ion implantation annealing (c), and 50-vacancy aggregation in Fe (d).

small energy-barriers. In Figures 6 and 7, we provide data characterizing all the bottleneck-events and all the events leading to lower-energy states in our runs, which agrees with the mechanisms illustrated in Fig. 4.

Fig. 6 presents the asymmetry of the large barrier events, i.e. the change in potential energy from the initial state to the final state. We define large barriers as those whose value is equal or greater than 90 % of the largest barrier encountered in all previous KMC steps. Negative asymmetry corresponds to relaxation, while a positive value means the barrier led to a final state with a potential energy greater than that of the initial state. We see that, while some of these high-barrier events directly lead to relaxation, most do not. These events are the bottleneck that limit relaxation to a logarithmic rate, but they do not generally directly produce relaxation.

Fig. 7 presents the activation barriers of the events that permitted sizable relaxation. We define these as events with a final state with a potential energy lower than that of the initial state by at margin of at least 0.2 eV for the Fe SIA system, 0.4 eV for Fe vacancies, 0.6 eV of Fe cascades and 0.5 eV for ion-implanted c-Si. These values were chosen to minimize the effect of fluctuations in energy at long timescales. These events, that directly lead to relaxation, have a distribution similar to that of all the other events, shown in Fig. 3.

As a whole Fig. 2 through Fig. 3 show that all these systems relax logarithmically through the *replenish and relax* mechanism. Indeed, the energy relaxation of the system progressively decelerates due to growing potential energy barriers that need to be crossed in order to access a section of the energy landscape where relaxation events are present. This distribution of relaxation events is emptied and the potential energy no longer decreases,

until an event with a large barrier is executed and replenishes it.

It is remarkable that these four different systems all lead to relaxation on logarithmic timescales, described by *replenish and relax*. Indeed, this indicates that such long-time structural evolution is not necessarily associated to complex materials, i.e. amorphous solids, colloids, glasses, polymers, but can be driven by the interaction of simple point defects in a pure cristal (all our configurations had more that 98% cristalline atoms). We also note that simulations in *a*-Si indicate logarithmic relaxation may appear after ion-implantation [58, 59].

V.   ATOMISTIC ASSESSMENT OF THE DRIVERS OF LOGARITHMIC RELAXATION

This apparently general behavior also raises the question as to the drivers of this type of annealing. Our simulations give a fully atomistic account of relaxation on logarithmic timescales over several orders of magnitude in time and should thus provide a much clearer picture, with less room for interpretation and speculation than previous studies. We focus on the Fe 50-vacancies and Fe 25-SIA cases, as the absence of recombination of point defects greatly simplifies the analysis.

We identified four elements that lead to relaxation over logarithmic timescales:

A.   Defect concentration heterogeneities

Vacancies are typically limited to one or two jumps before aggregating, which promotes large cluster formation in high-density areas. Because SIA-clusters can execute long jumps, this effect is much weaker. Fig. 8 quantifies this effect, which is in agreement with visual inspection (see e.g. the movies in the Supplemental Material [57]). We identified the size and the center of mass (CoM) of each defect cluster at the end of each simulation and calculated the density of defects that were present in the neighborhood of the CoM in the local initial configuration, using gaussian kernel averaging. In the case of the 50-vacancy system, 57 % of the size of the final clustered can be explained by the initial density of defects, while it explains less than 20 % in the 25-SIA system. We infer that the heterogeneity in the initial density of defects leads to a distribution of clusters of different sizes, which each have their own distribution of barriers to *replenish* the potential energy landscape. On aggregate, this will lead to a wide distribution of such barriers. This is in general agreement with the Gibbs model and its variations. This effect seems important in the vacancy case, but weak in the interstitial case.
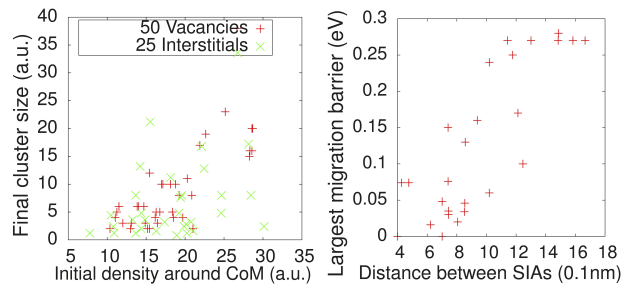

FIG. 8. Left panel: the size of the clusters in the final configuration after the 50-vacancy (R^2=0.58) and 25-SIA (R^2=0.14) simulations as a function of the initial density of point defects in the neighborhood of their CoM. Right panel: The largest barrier crossed when two SIAs set at a given distance from each other aggregate (R^2=0.69).

B.   Concentration-enhanced mobility

In the first stages of relaxation, the systems contains an important density of mobile point defects and point defect clusters, which decreases as the system evolves. In Fig. 3, we observe that relaxation occurs with barriers lower than that of diffusion of isolated point defects and isolated point defect clusters. This corresponds to 0.3 eV for SIAs and 0.64 eV for mono-vacancies [44] (di- and tri-vacancies are know to diffuse slightly faster). This indicates that mobility is enhanced in the first stages of relaxation. For vacancies, it is known that interactions between nearby vacancies can lead to low-barrier vacancy jumps and that this effect is stronger when distances are shorter [35, 60]. In Fig. 8, we show that high local concentration of SIAs also leads to high mobility. In other words, migration is enhanced by defect proximity and concentration. During relaxation, as the cluster size increases and potential energy decreases, the distance between mobile point defects increases and activation barriers increase. This is a mechanism in general agreement with Eyring-like models.

C.   Cluster-size dependent bonding energies

Diffusivity of large vacancy clusters (tetra-vacancies and larger) decreases with cluster size and thermal lifetimes increase with cluster size [35]. Thus, as the clusters grow in size, one would expect the overall relaxation-limiting barriers to increase. This mechanism observed for the vacancy case is in general agreement with Eyring-like models.

In the case of SIA-clusters, the relationship is not well defined. SIAs bind in a large number of metastable sessile and glissile configurations [30, 61]. The activation barriers that lead to reconfiguration and interactions with nearby defects are unpredictable and largely independent of cluster size [62, 63], especially since the configurations are generated through off-equilibrium dynamics. Both
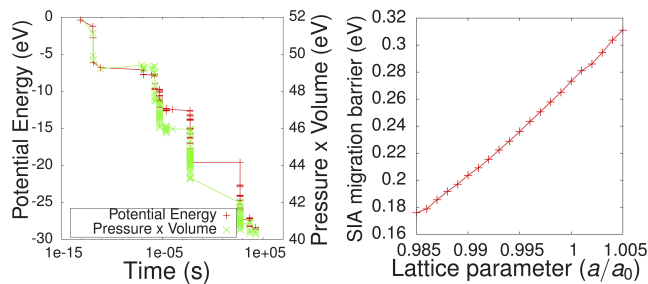
FIG. 9. Left panel: the hydrostatic pressure of the 25-SIA system and its potential energy as a function of time. Right panel: the effect of hydrostatic pressure on SIA mobility.

FIG. 10. Time evolution of potential energy for the aggregation of 25 SIAs in Fe, with the A04 potential.

visual inspection of simulations and the data presented in the left panel of Fig. 8 indicate that mobility is weakly, if at all, related to cluster size during these simulations.

D. Defect-induced pressure

In our NVT runs, aggregation of point defects relieved pressure. In the left panel of Fig. 9, we show the typical evolution of the total pressure, computed as the sum of all the traces of the atomic virial stress tensors, for the 25-SIA system. The aggregation of SIAs leads to a large decrease in hydrostatic stress, which follows the relaxation in potential energy very closely. Shear stresses, including the Von Mises stress, are an order of magnitude smaller and, moreover, do not have a systematic trend during relaxation. We assessed the impact of pressure on SIA mobility by measuring the activation barrier for a SIA in a box with various lattice-parameters. The results are plotted in the right panel of Fig. 9. We see that 1% compressive hydrostatic strain leads to a 26% decrease in barrier energy for the M07 potential. Thus, when the system is unrelaxed, mobility is enhanced through pressure. As the system relaxes, this effect decreases, causing the barriers to increase towards their unstrained value. We note that in the A04 potential, the effect of pressure on mobility is much smaller, a 1% compressive hydrostatic strain leads to a 7% decrease of the activation barrier.

For mono-vacancies, the effect of stress on diffusion is small. A 1% tensile hydrostatic strain leads to a 6% increase of the activation energy, both in the A04 and M07 potential, which means that the tensile strain release during relaxation accelerates time-evolution, albeit by a small quantity compared to the other effects.

In other words, the interplay between the overall pressure in the system, the state of relaxation and mobility plays an important role to logarithmically limit the time-evolution of SIA aggregation as described by the M07 potential, in general agreement with Eyring-like models, but plays a much smaller role if this process is described with the A04 potential. In the vacancy case, the effect is very small and in fact plays against logarithmic relaxation.
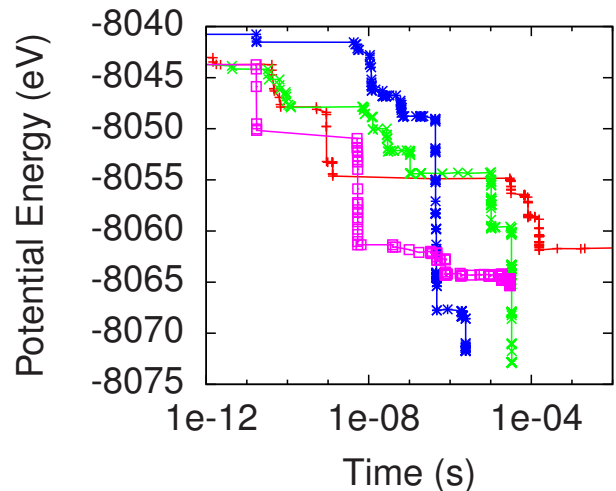
We also looked at variations in pressure during events corresponding to bottlenecks. We saw no clear relationship between the pressure change from the initial state to the saddle point and the activation barrier, which indicates that the model of Ref. [21] does not apply to these simple point-defect systems.

VI. CONCLUSION

To conclude, through the use of SEAKMC and k-ART simulations, we found that simple point-defect interactions can lead to relaxation on logarithmic timescales described by the *replenish and relax* process. We showed three examples in Fe and one in *c*-Si that fit this description. For the simplest cases, the aggregation of 50 vacancies in Fe and the aggregation of 25 interstitial in Fe, we identified four atomistic mechanisms explaining how the barriers to relaxation increase as the system relaxes: defect concentration heterogeneities, concentration-enhanced mobility, cluster-size dependent bonding energies and defect-induced pressure. Some of these mechanisms support the Gibbs model of relaxation, while others give credence to variations of the Eyring model.

The variety of mechanisms involved in these seemingly simple problems is striking. It is also clear that slow relaxation is caused by events localized around interacting defects. Furthermore, this work provides a framework, based on accelerated atomistic simulations, to approach more complex problems, that may well share common mechanisms with point defect kinetics. This may not necessarily be the case, but the generality of our observations motivate such further investigation.
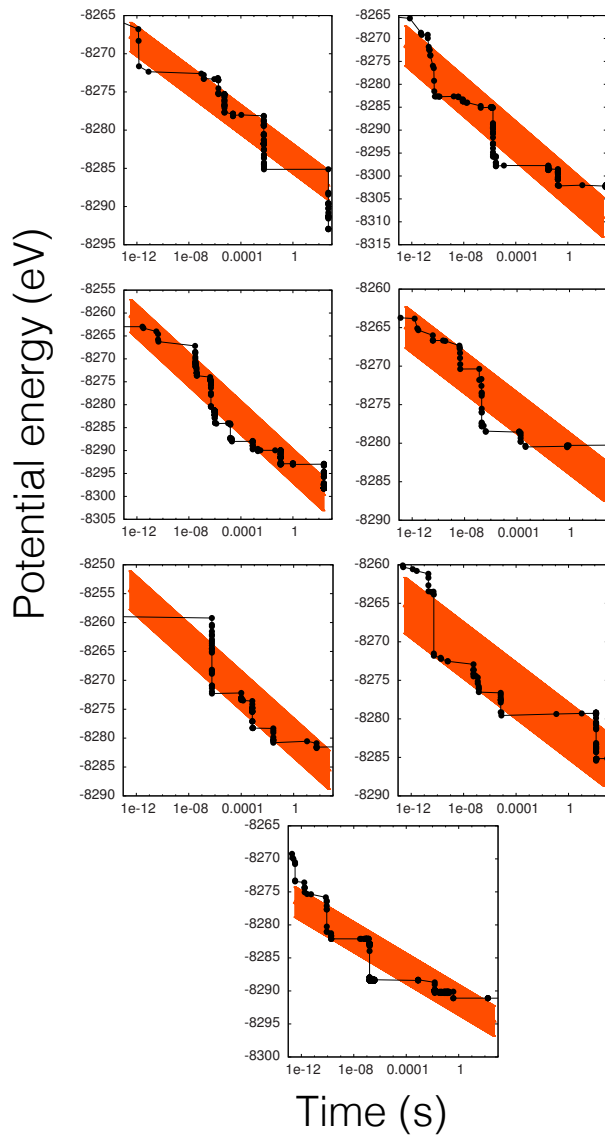
FIG. 11. The potential energy for each 25 interstitial run with the M07 potential. The fits to logarithmic relaxation and its confidence interval are in orange.

Appendix A: Interstitial aggregation using Ackland 2004 potential

Fig. 10 shows SIA aggregation runs done using the Ackland 2004 potential. Overall, the general features are similar to the runs performed with the Marinica 2007 potential, although the drops in energy are more pronounced.

Appendix B: Log-linear fits to SIA simulations

Figure 11 illustrates the nature of the slow, time-dependent behavior which we call logarithmic relaxation. The figure includes the results of seven individual simulations showing how the potential energy evolves in a 2025 atom system than initially contains 25 mono-interstitials. As the interstitials migrate and form small clusters, the potential energy correspondingly declines in a manner that produces approximately linear behavior on the semi-logarithmic plots. Relaxation that follows a non-linear trend, but that still takes place over long times is also referred to as logarithmic relaxation in this paper.

ACKNOWLEDGMENTS

[1] W. Götze and M. Sperl, Physical Review E **66**, 011405 (2002).
[2] V. Orlyanchik and Z. Ovadyahu, Physical review letters **92**, 066801 (2004).
[3] A. Amir, Y. Oreg, and Y. Imry, Proceedings of the National Academy of Sciences **109**, 1850 (2012).
[4] O. Manyuhina, A. Fasolino, and M. Katsnelson, Polymer **48**, 4849 (2007).
[5] M. Sperl, Physical Review E **68**, 031405 (2003).
[6] M. Sperl, Physical Review E **71**, 060401 (2005).
[7] E. Zaccarelli, Journal of Physics: Condensed Matter **19**, 323101 (2007).
[8] C. E. Colosqui, J. F. Morris, and J. Koplik, Physical review letters **111**, 028302 (2013).
[9] H. Yang, G. Luo, P. Karnchanaphanurach, T.-M. Louie, I. Rech, S. Cova, L. Xun, and X. S. Xie, Science **302**, 262 (2003).
[10] M. Lagi, P. Baglioni, and S.-H. Chen, Physical review letters **103**, 108102 (2009).
[11] K. Kämpf, F. Klameth, and M. Vogel, The Journal of chemical physics **137**, 205105 (2012).
[12] O. Ronsin, C. Caroli, and T. Baumberger, Physical review letters **103**, 138302 (2009).
[13] A. Knoll, D. Wiesmann, B. Gotsmann, and U. Duerig, Physical review letters **102**, 117801 (2009).
[14] O. Tsiok, V. Brazhkin, A. Lyapin, and L. Khvostantsev, Physical review letters **80**, 999 (1998).

[15] K. Trachenko, V. Brazhkin, O. Tsiok, M. T. Dove, and E. Salje, Physical Review B **76**, 012103 (2007).

[16] M. Vandamme and F.-J. Ulm, Proceedings of the National Academy of Sciences **106**, 10552 (2009).

[17] E. Masoero, H. Manzano, E. Del Gado, R. Pellenq, F. Ulm, and S. Yip, Mechanics and Physics of Creep, Shrinkage, and Durability of Concrete@ sA Tribute to Zdenk P. Bazant , 166 (2013).

[18] H. Eyring, The Journal of chemical physics **4**, 283 (1936).

[19] J. Brey and A. Prados, Physical Review E **63**, 021108 (2001).

[20] B. Huisman and A. Fasolino, Physical Review E **74**, 026110 (2006).

[21] K. Trachenko, Physical Review B **75**, 212201 (2007).

[22] A. Knoll, D. Wiesmann, B. Gotsmann, and U. Duerig, Physical Review Letters **103**, 119802 (2009).

[23] M. Gibbs, J. Evetts, and J. Leake, Journal of Materials Science **18**, 278 (1983).

[24] R. S. Crandall, Physical Review B **43**, 4057 (1991).

[25] P. Roura and J. Farjas, Physical review letters **103**, 119801 (2009).

[26] P. Roura and J. Farjas, Acta Materialia **57**, 2098 (2009).

[27] M. A. Lomholt, L. Lizana, R. Metzler, and T. Ambjörnsson, Physical Review Letters **110**, 208301 (2013).

[28] L. K. Béland, Y. Anahory, D. Smeets, M. Guihard, P. Brommer, J.-F. Joly, J.-C. Pothier, L. J. Lewis, N. Mousseau, and F. Schiettekatte, Physical Review Letters **111**, 105502 (2013).

[29] F. El-Mellouhi, N. Mousseau, and L. J. Lewis, Physical Review B **78**, 153202 (2008).

[30] L. K. Béland, P. Brommer, F. El-Mellouhi, J.-F. Joly, and N. Mousseau, Physical Review E **84**, 046704 (2011).

[31] L. K. Béland and N. Mousseau, Physical Review B **88**, 214201 (2013).

[32] H. Blythe, physica status solidi (a) **17**, 293 (1973).

[33] P. Brommer and N. Mousseau, Physical Review Letters **108**, 219601 (2012).

[34] H. Xu, R. E. Stoller, and Y. N. Osetsky, Journal of Nuclear Materials **443**, 66 (2013).

[35] P. Brommer, L. K. Béland, J.-F. Joly, and N. Mousseau, Physical Review B **90**, 134109 (2014).

[36] G. K. N'Tsouaglo, L. K. Béland, J.-F. Joly, P. Brommer, N. Mousseau, and P. Pochet, "Probing potential energy surface exploration strategies for complex systems," (2014), arXiv:1407.7371.

[37] C.-C. Fu, J. Dalla Torre, F. Willaime, J.-L. Bocquet, and A. Barbu, Nature materials **4**, 68 (2004).

[38] W. Brostow and J. Kubát, Physical Review B **47**, 7659 (1993).

[39] G. Luo, I. Andricioaei, X. S. Xie, and M. Karplus, The Journal of Physical Chemistry B **110**, 9363 (2006).

[40] M. Warren and J. Rottler, Physical Review E **76**, 031802 (2007).

[41] H. Xu, Y. N. Osetsky, and R. E. Stoller, Physical Review B **84**, 132103 (2011).

[42] H. Xu, Y. N. Osetsky, and R. E. Stoller, Journal of Physics: Condensed Matter **24**, 375402 (2012).

[43] H. Xu, R. E. Stoller, Y. N. Osetsky, and D. Terentyev, Physical review letters **110**, 265503 (2013).

[44] L. Malerba, M. Marinica, N. Anento, C. Björkas, H. Nguyen, C. Domain, F. Djurabekova, P. Olsson, K. Nordlund, A. Serra, *et al.*, Journal of Nuclear Materials **406**, 19 (2010).

[45] N. Mousseau, L. K. Béland, P. Brommer, J.-F. Joly, F. El-Mellouhi, E. Machado-Charry, M.-C. Marinica, and P. Pochet, Journal of Atomic, Molecular, and Optical Physics **2012** (2012).

[46] J.-F. Joly, L. K. Béland, P. Brommer, F. El-Mellouhi, and N. Mousseau, Journal of Physics: Conference Series **341**, 012007 (2012).

[47] J.-F. Joly, L. K. Béland, P. Brommer, and N. Mousseau, Physical Review B **87**, 144204 (2013).

[48] H. Jiang, C. Jiang, D. Morgan, and I. Szlufarska, Computational Materials Science **89**, 182 (2014).

[49] A. B. Bortz, M. H. Kalos, and J. L. Lebowitz, Journal of Computational Physics **17**, 10 (1975).

[50] B. D. McKay *et al.*, *Practical graph isomorphism* (Department of Computer Science, Vanderbilt University, 1981).

[51] B. D. McKay, Computer Science Dept., Australian National University (2007).

[52] G. Barkema and N. Mousseau, Physical review letters **77**, 4358 (1996).

[53] R. Malek and N. Mousseau, Physical Review E **62**, 7723 (2000).

[54] E. Machado-Charry, L. K. Béland, D. Caliste, L. Genovese, T. Deutsch, N. Mousseau, and P. Pochet, The Journal of chemical physics **135**, 034102 (2011).

[55] L. K. Béland, E. Machado-Charry, P. Pochet, and N. Mousseau, Physical Review B **90**, 155302 (2014).

[56] G. Ackland, M. Mendelev, D. Srolovitz, S. Han, and A. Barashev, Journal of Physics: Condensed Matter **16**, S2629 (2004).

[57] L. Béland, Y. Osetskiy, R. Stoller, and H. Xu, Supplemental Material **1**, 1 (2014).

[58] J.-C. Pothier, F. Schiettekatte, and L. J. Lewis, Physical Review B **83**, 235206 (2011).

[59] J.-F. Joly, "Étude sur la cinétique des défauts structuraux dans le silicium amorphe." (2013).

[60] V. Kapinos, Y. N. Osetskii, and P. Platonov, Journal of Nuclear Materials **184**, 221 (1991).

[61] M.-C. Marinica, F. Willaime, and N. Mousseau, Physical Review B **83**, 094119 (2011).

[62] D. Terentyev, L. Malerba, and M. Hou, Physical Review B **75**, 104108 (2007).

[63] N. Anento, A. Serra, and Y. N. Osetsky, Modelling and Simulation in Materials Science and Engineering **18**, 025008 (2010).